



## Supporting Information

for *Small*, DOI: 10.1002/sml.201905611

An Integrated Plasmo-Photoelectronic Nanostructure  
Biosensor Detects an Infection Biomarker Accompanying Cell  
Death in Neutrophils

*Younggeun Park, Byunghoon Ryu, Qiufang Deng, Baihong  
Pan, Yujing Song, Yuzi Tian, Hasan B. Alam, Yongqing Li,\*  
Xiaogan Liang,\* and Katsuo Kurabayashi\**

Supporting Information

**An integrated plasmo-photoelectronic nanostructure biosensor detects an infection biomarker accompanying cell death in neutrophils**

*Younggeun Park, Byunghoon Ryu, Qiufang Deng, Baihong Pan, Yujing Song, Yuzei Tian, Hasan B. Alam, Yongqing Li,\* Xiaogan Liang,\* and Katsuo Kurabayashi\**

(Dr. Y. Park, B. Ryu, and Dr. Q. Deng are equally contributed.)

Dr. Y. Park, B. Ryu, Y. Song, Prof. X. Liang, Prof. K. Kurabayashi  
Department of Mechanical Engineering, University of Michigan, Ann Arbor MI, 48109 USA  
E-mail: xiaoganl@umich.edu, katsuo@umich.edu

Dr. Y. Park, Prof. Y. Li, Prof. X. Liang, Prof. K. Kurabayashi  
Center for Integrative Research in Critical Care, University of Michigan, Ann Arbor MI, 48109 USA  
E-mail: yqli@med.umich.edu, xiaoganl@umich.edu, katsuo@umich.edu

Dr. Q. Deng, Dr. B. Pan, Y. Tian, Prof. H. Alam, Prof. Y. Li  
Department of Surgery, University of Michigan, Ann Arbor MI, 48109 USA  
E-mail: yqli@med.umich.edu

Dr. Q. Deng  
Department of Endocrinology, Endocrinology Research Center, The Xiangya Hospital of Central South University, Changsha, Hunan 410008, China

Dr. B. Pan, Y. Tian  
Department of General Surgery, The Xiangya Hospital of Central South University, Changsha, Hunan 410008, China

## Experimental details

*Au nanoparticle array synthesis and characterization:* Arrayed AuNHs were fabricated as the surface parts of the Bio-NOF layer by controlling the surface energy using block copolymer (BCP) chemistry. After a cleaning process, a thin SiO<sub>2</sub> layer was coated with PS-*b*-P2VP solution to control the surface energy. An Au nanolayer was deposited onto the BCP-treated SiO<sub>2</sub> substrate in vacuum at room temperature in an electron-beam evaporator system (Angstrom Engineering Evovac Evaporator). Thermal treatment of the substrate was followed by an annealing process with air condition. Then the morphology and density of the formed AuNH arrays were characterized by scanning electron microscopy (Hitachi SU-8000) and Image J software.

*Few-layer MoS<sub>2</sub> photodetector channel fabrication:* A few-layer MoS<sub>2</sub> photoconductive channel was first prepared on a SiO<sub>2</sub>/Si substrate using a micro-printing.<sup>[1]</sup> A Ti (5 nm) - Au (50 nm) electrode pair providing the drain and source contacts for the MoS<sub>2</sub> channel was subsequently fabricated by metal deposition and lift-off. The topography of the MoS<sub>2</sub>

*Integration of AuNH-deposited Bio-NOF layer and few-layer MoS<sub>2</sub> photoconductive channel:* The AuNH-deposited Bio-NOF layer and the atomically layered MoS<sub>2</sub> photoconductive channel were first prepared separately. Subsequently, these components were integrated into a single on-chip device platform. Based on macro-manipulation control, AuNH-deposited Bio-NOF layer was placed on the Au electrodes next to the MoS<sub>2</sub> channel. Using a microscope along with alignment marks on the substrates of the Bio-NOF and MoS<sub>2</sub> channel, these components were assembled. They were physically bonded using a biomedical double-sided adhesion layer (100 μm) handling.

*Near-field electromagnetic radiation calculation:* Near-field electromagnetic radiation around an AuNH particle was simulated by solving the Helmholtz wave equation:  $\nabla \times (\mu_r^{-1} \nabla \times E) -$

$k_0^2(\epsilon_r - j\sigma\omega\epsilon_0)E = 0$  with a finite element analysis method (FEA, COMSOL Multiphysics software). Hybrid mesh structures were created for the AuNH particle to adopt its round shape. The relative permeability and complex permittivity of gold were assumed to be  $\mu_r = 1$  and  $\epsilon_r = f(\lambda)$ , respectively. The polarization vector was applied in the direction parallel to the AuNH, whereas the direction of the k-vector was taken to be perpendicular to the plane of the structure. Perfect absorption was assumed at the outer boundary to minimize spurious reflections by setting a perfectly matched layer and an integration layer in the concentric space. The dimension of the AuNH ( $d_{AuNH} = 40$  nm) was chosen based on the SEM images.

Enzyme-linked sandwich assay (ELISA): ELISA is the current gold standard method to quantify CitH3 in a serum sample. A 96-well plate of CitH3 ELISA kit was developed in our laboratory as described previously.<sup>[2]</sup> Briefly, an anti-CitH3 monoclonal antibody (Cayman Chemical, Ann Arbor, MI) was coated onto a 96-well plate as a capture antibody, then the plates were blocked with a blocking buffer (Thermo Scientific, Rockford, IL, USA) at room temperature (RT) for 2 h. Serum was treated with DNase. And it added to the wells with an 80  $\mu$ l blocking buffer and incubated at RT for 2 h. After 4 times of washing, an anti-CitH3 rabbit polyclonal antibody (Abcam, Cambridge, MA, USA) was added as a detecting antibody and incubated at RT for 2 h. Following 4 times of washing, the anti-rabbit peroxidase-labeled secondary antibody was incubated in wells at room temperature for 1 h. After removing extra secondary antibodies with 4 thorough washes, we treated the plate with 3, 3', 5, 5'-Tetramethylbenzidine (TMB) for 20 minutes in dark followed by stop solution (R&D Systems Inc., Minneapolis, MN, USA). We determined CitH<sub>3</sub> levels by measuring absorbance at  $\lambda = 450$  nm.

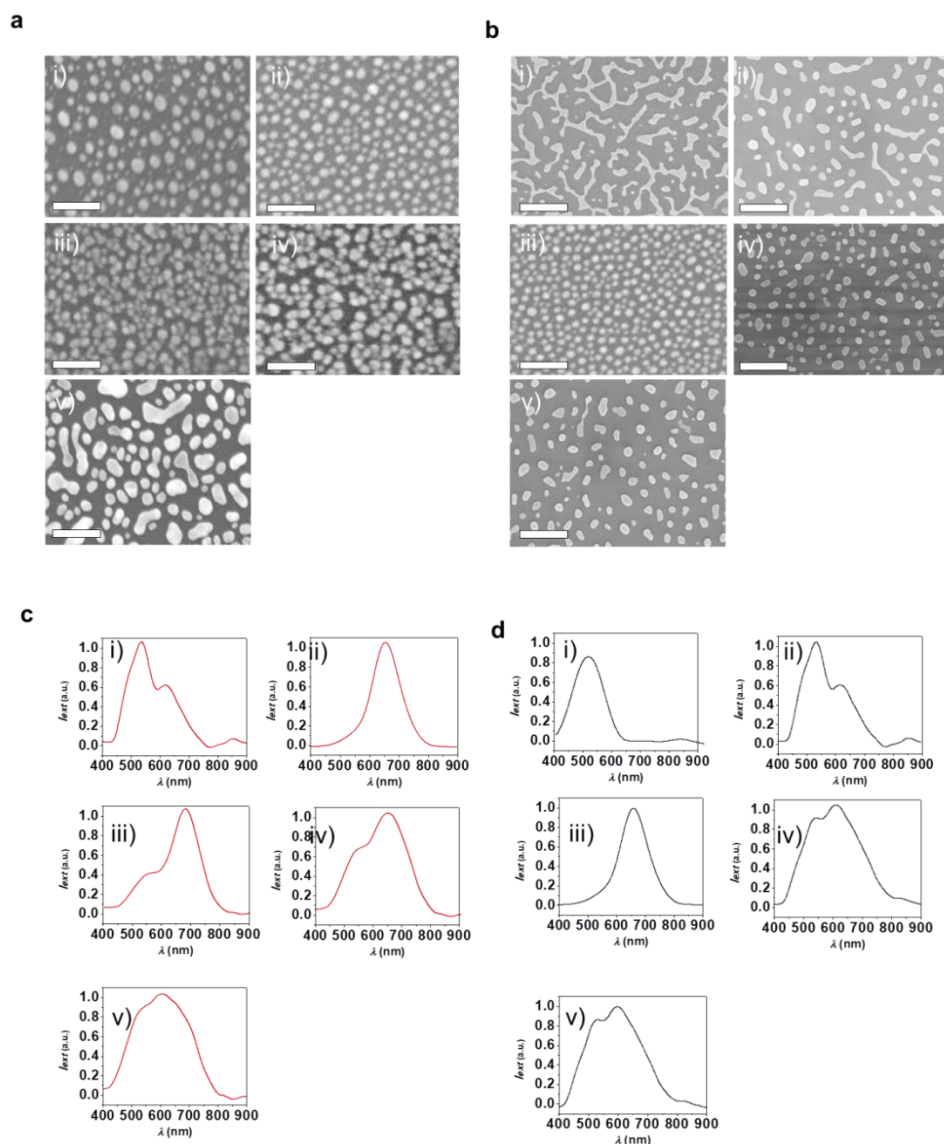


**Figure S1. Fabrication and characterization of arrayed plasmonic gold nano hemispheres (AuNHs).** The arrayed AuNHs were constructed in a controlled manner by varying the gold layer deposition thickness and the thermal treatment duration. (a) AuNH morphologies (SEM images) resulting from a Au layer deposited with the thickness of 2, 5, 10, 20, and 40 nm, respectively, (scale bar = 250 nm) under the thermal treatment of 30 min at  $T = 500$  °C. (b) AuNH morphologies (SEM images) resulting from the thermal treatment of 10, 30, 60, and 120 min, respectively, at  $T = 500$  °C for a Au layer deposited with the thickness of 5 nm (scale bar = 250 nm). (c) LSPR extinction spectra of AuNHs fabricated with a Au layer deposited with the thickness of 2, 5, 10, 20, and 40 nm, respectively, (scale bar = 250 nm) under the thermal treatment of 30 min at  $T = 500$  °C. and (d) LSPR extinction spectra of AuNHs with a Au layer deposited with the thickness of 5 nm under the thermal treatment of 10, 30, 60, and 120 min, respectively, at  $T = 500$  °C (scale bar = 250 nm).

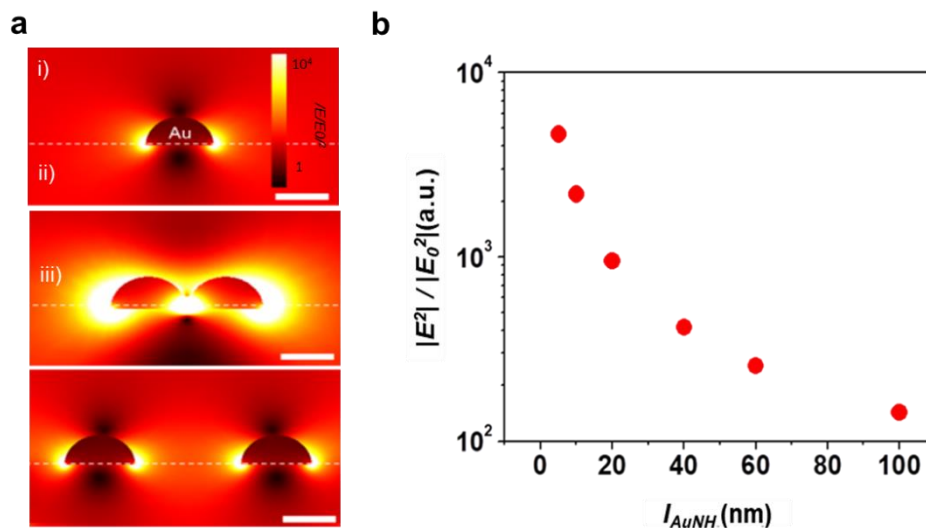


**Figure S2. Finite element analysis (FEA) of AuNH LSPR substrate.** A) near-field electromagnetic field distributions around i) a single and two neighboring AuNHs with  $I_{inter} =$  ii) 10 nm and iii) 100 nm at  $\lambda = 650$  nm (scale bar = 50nm) and E-field enhancement as a function of  $I_{AuNH}$ .

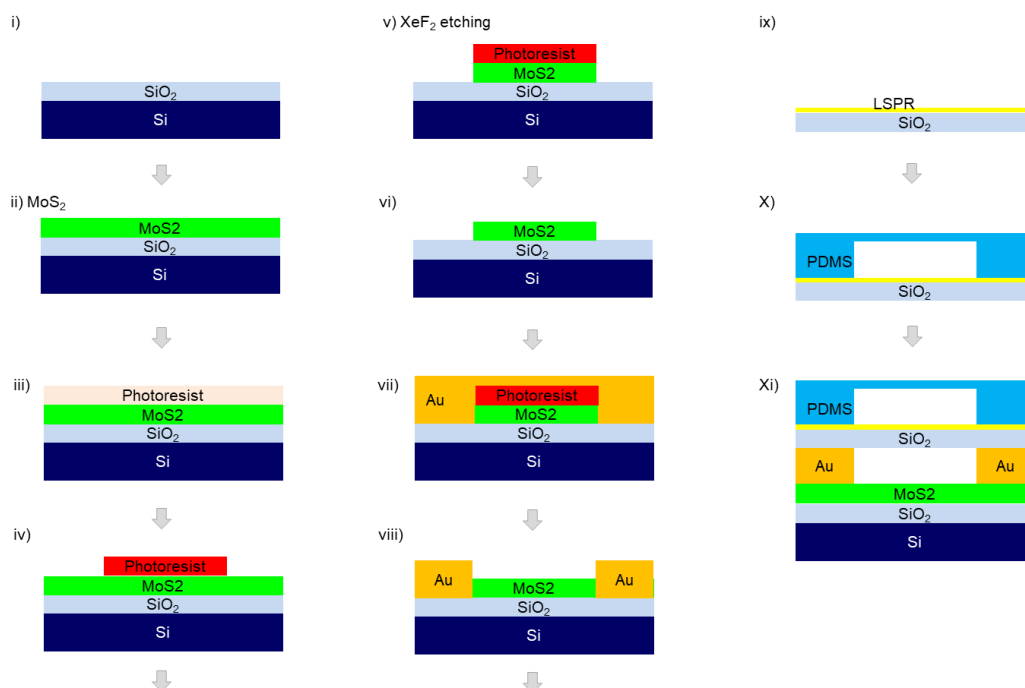


**Figure S3. Fabrication and integration of few-layer MoS<sub>2</sub> channel for the iNOBS device.**

i)-ii) A few-layer MoS<sub>2</sub> channel was patterned on a thermally oxidized Si substrate using a micro-printing method. iii)-viii) Using photolithography followed by metal deposition and lift-off, we deposited a pair of Ti (5 nm)/Au (50 nm) electrodes that serve as drain and source contacts for the MoS<sub>2</sub> photoconductive channel. ix) In the meantime, we fabricated a nanoplasmonic optical window layer by forming AuNH arrays on a thin (100  $\mu\text{m}$ -thick) SiO<sub>2</sub> substrate. x) The microfluidic well chamber made of PDMS was attached on the AuNH/SiO<sub>2</sub> Bio-NOF layer (prior to antibody functionalization) after oxygen plasma surface treatment of PDMS. xi) The microfluidics/Bio-NOF unit was integrated on the MoS<sub>2</sub> channel. Using a micro-manipulator, we placed the unit on the Au electrode of the MoS<sub>2</sub> detection platform. Here, we used photolithographically patterned alignment marks to precisely align the features on the AuNH/SiO<sub>2</sub> Bio-NOF layer and the MoS<sub>2</sub> channel-patterned Si substrate and bonded them together using a biomedical double-sided adhesion layer (100  $\mu\text{m}$ ).

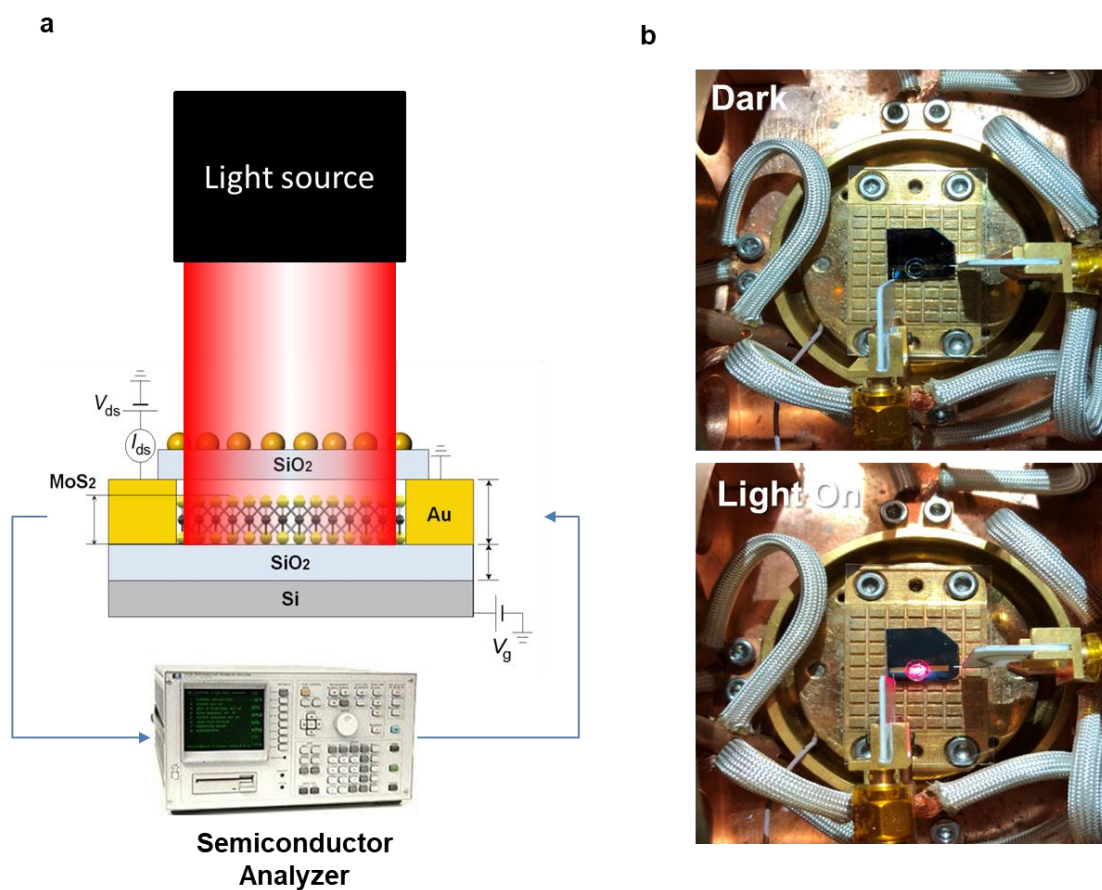


**Figure S4. Schematic design (a) and photos (b) of whole device setup for the measurement.**



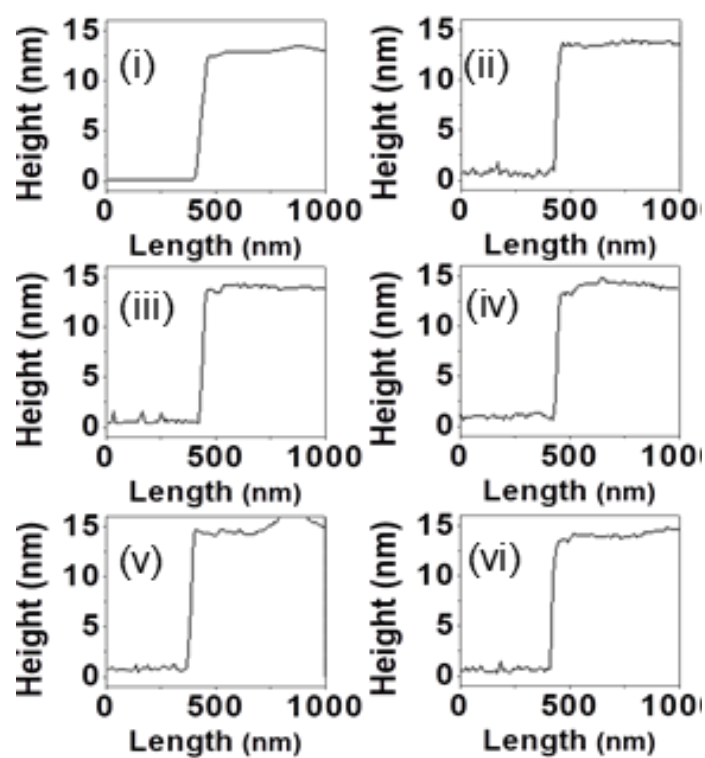


**Figure S5.** Morphology of the few-layer MoS<sub>2</sub> channel. Cross-sectional profiles along the white lines from (i) to (vi) of the atomic force microscope image of MoS<sub>2</sub> layer on a SiO<sub>2</sub> layer in **Figure 3b**.

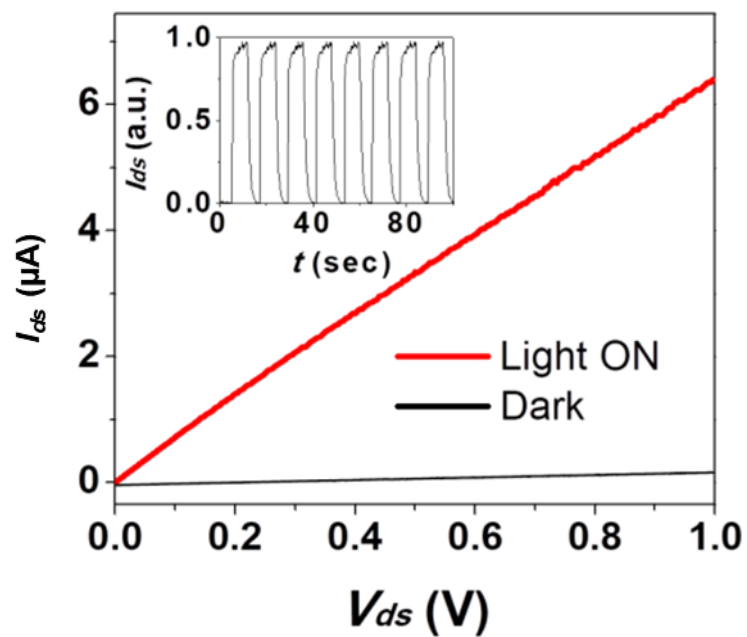


**Figure S6.**  $I_{ds}$ - $V_{ds}$  characteristics of the MoS<sub>2</sub> under the dark condition and the light illumination ( $\lambda = 650$  nm and  $P = \sim 2.4$  mW) (Inset:  $I_{ds}$  under alternating Light-ON and OFF states).

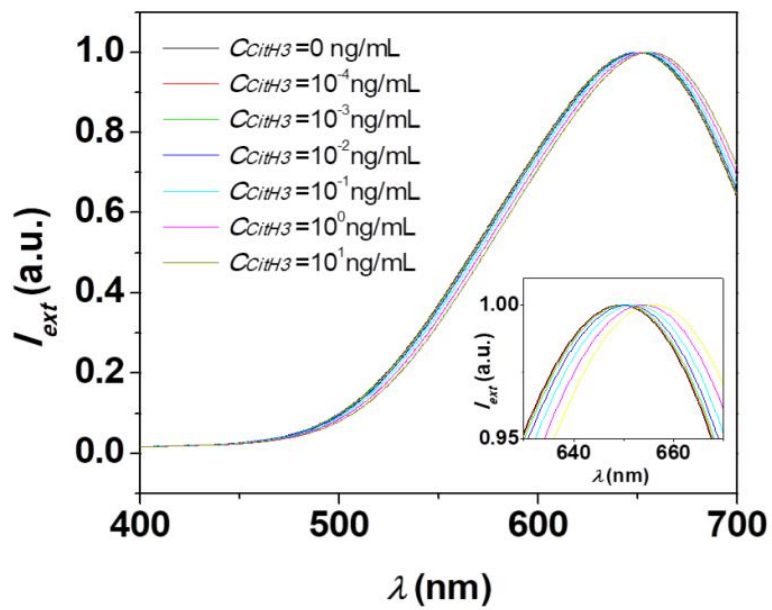


**Figure S7.** LSPR spectral peak shift of the antibody-conjugated Bio-NOF layer with varying  $C_{CitH3}$ .

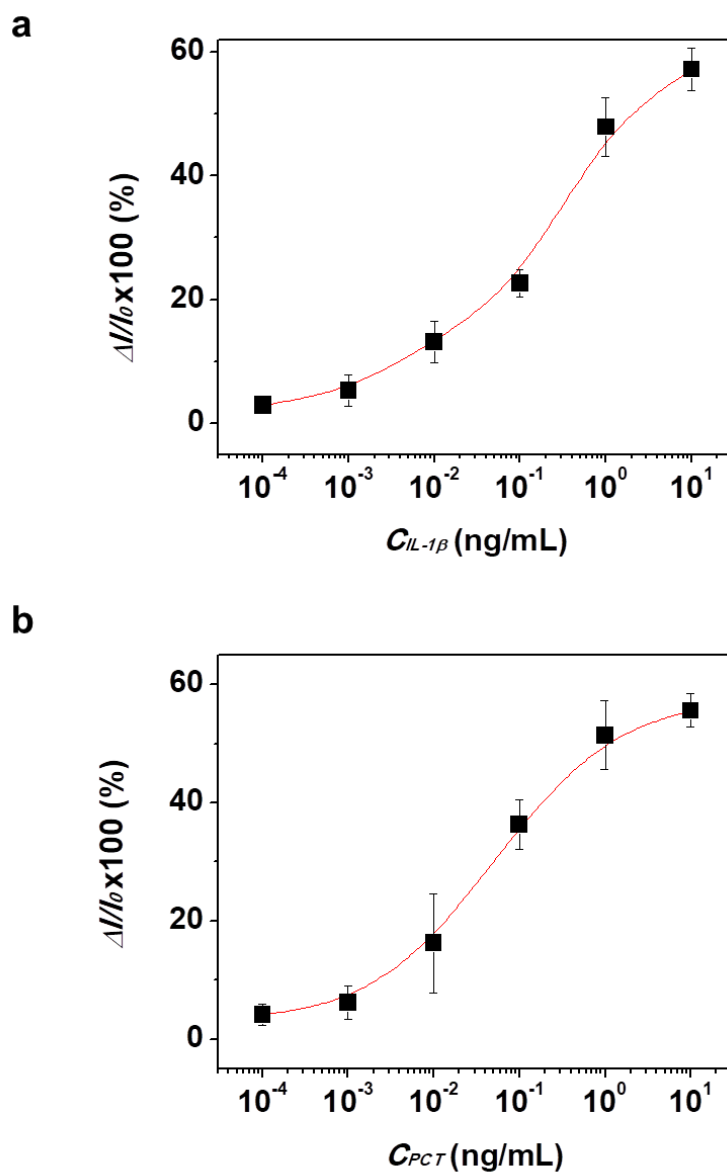


**Figure S8. Calibration curves of (a)  $C_{IL-1\beta}$  and (b)  $C_{PCT}$  in sham.** The value of  $\Delta I/I_0 \times 100$  represents the photocurrent variation in % at 10 min. All the detections were performed at  $\lambda = 650\text{nm}$  and  $P = 2.4 \text{ mW/cm}^2$ . The estimated  $K_d$  values are 0.572 ng/mL, 0.717 ng/mL, and 0.658 ng/mL for CitH3, PCT, and IL-1 $\beta$ , respectively.

**Table S1. Photoresponsivity.**

Sample	Measurement conditions	Photoresponsivity
Ref. 1 <sup>[3]</sup>	$V_g = -70$ V, $V_{ds} = 8$ V $\lambda = 561$ nm, $P = 150$ pW	$\sim 880$ A $W^{-1}$
Ref. 2 <sup>[4]</sup>	$V_g = 37$ V, $V_{ds} = 2$ V White illumination, $P = 0.7$ mW	$\sim 11.4$ mA $W^{-1}$
Ref. 3 <sup>[5]</sup>	$V_g = -40$ V, $V_{ds} = 1$ V $\lambda = 520$ nm, $P = 40$ mW	$\sim 0.25$ A $W^{-1}$
Ref. 4 <sup>[6]</sup>	$V_g = -3$ V, $V_{ds} = 1$ V $\lambda = 633$ nm, $P = 50$ mW	$\sim 12$ mA $W^{-1}$
Ref. 5 <sup>[7]</sup>	$V_g = 0$ and $50$ V, $V_{ds} = 1$ V $\lambda = 550$ nm, $P = 80$ $\mu$ W	$\sim 50$ $\mu$ A $W^{-1}$ (at $V_g = 0$ ) $\sim 7.5$ mA $W^{-1}$ (at $V_g = 50$ )
Our MoS <sub>2</sub>	$V_g = 0$ V, $V_{ds} = 1$ V $\lambda = 650$ nm, $P = 24$ nW	$\sim 267$ A $W^{-1}$

To demonstrate that our device can be a portable and simple biosensor for point-of-care (POC) applications, we operated it at a relatively lower drain voltage ( $V_{ds} = 1$  V) with no gate bias voltage ( $V_g = 0$  V).

**LSPR structures**

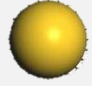
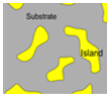







Plasmon resonances are extremely sensitive to the refractive index of the surrounding medium.

With the value of the refractive index increased, the LSPR peak shows a red shift. The plasmon resonance sensitivity is given by  $d\lambda/dn$ , where  $d\lambda$  is the shift of the resonance peak wavelength, and  $dn$  is the change in the refractive index. Previous studies explored various approaches to achieve a higher sensitivity value, a large figure of merit (FOM), and a lower limit of detection (LOD) for LSPR sensing. Each of these studies employed a relatively simple LSPR structure fabrication method applied for a large substrate area.

**Table S2. Sensitivity of plasmonic structures.** The figure of merit (FOM) was estimated by measuring the LSPR peak wavelength shift range as the refractive index  $n_m$  was varied from 1.33 to 1.47.

$\Delta\lambda$	RIU	FWHM	FOM
42	300	125	2.40

**Table S3. Comparison of LSPR substrate\***

	Shape	Method	FOM	Uniformity	Substrate Size
AuNPs <sup>[8]</sup>		Drop-cast	1-1.5	Low	10 mm <sup>2</sup>
Island <sup>[9]</sup>		Dewetting	0.50-1.1	Medium	10 mm <sup>2</sup>
Nano Ring <sup>[10]</sup>		Colloidal lithography	2.1	Very Low	0.25 mm <sup>2</sup>
Nano Disk <sup>[10]</sup>		Colloidal lithography	2.7	Very Low	0.25 mm <sup>2</sup>
Nano Disk <sup>[11]</sup>		Nanoimprint Lithography	1.635	High	10 mm <sup>2</sup>
Nano Disk <sup>[12, 13]</sup>		Electron Beam Lithography	2.0	High	0.25 mm <sup>2</sup>
Fano-Type Partially fill <sup>[14]</sup>		Theory	0.73		
Fano-Type Fully fill <sup>[14]</sup>		Theory	2.22		
Au NanoStar <sup>[15, 16]</sup>		Drop-cast	0.19 - 1.26	Very Low	5 mm <sup>2</sup>

\* This table does not include colloidal particles in solution.

In Table S3, we compare various substrate-bound nanoplasmonic structures used for LSPR sensing in previous studies. The compared features of each structure include the fabrication method, figure of merit (FOM), structural uniformity, and substrate size. The FOM of 2.4 for the arrayed AuNH structure in this paper is close to the highest value of 2.7 reported in the literature.

**Table S4. Limit of detection (LOD) resulting from different CitH3 detection methods.**

We experimentally determined LOD values for the three methods used in the current study to detect CitH3 in serum. Here, the LOD value is given by  $3\sigma/k_{slope}$ , where  $\sigma$  is the standard deviation of the background noise detected with a blank sample, and  $k_{slope}$  is the regression slope extracted by sigmoidal curve-fitting to the standard curve.

	<b>Sample Volume (<math>\mu\text{L}</math>)</b>	<b>Blank S.D. (<math>\sigma</math>) (%)</b>	<b>U<sub>system</sub> (<math>3\sigma</math>) (%)</b>	<b>k slope (<math>\text{pg/mL}</math>)-1</b>	<b>LOD=<math>3\sigma/k_{slope}</math> (<math>\text{pg/mL}</math>)</b>
iNOBS <sup>1</sup>	2.5	0.00093	0.00280	0.0032	0.87
LSPR	25	0.00236	0.00709	0.0004	17.28
ELISA <sup>2</sup>	150	0.0155	0.0405	0.00175	232

<sup>1</sup> The LOD of iNOBS in PBS was 0.14 which was lower than that in sham.

<sup>2</sup> The claimed LOD of the ELISA kit was 100 pg/mL from the company and our own signal intensity was a slightly lower than the company's data, and that is why we obtained the higher LOD than expected.



**Table S5. Estimated LOD for IL-1 $\beta$  and PCT in sham mice serum using the iNOBS device.** We experimentally determined the LOD values for the three sepsis-related biomarkers in serum samples from sham mice.

	<b>Blank S.D.</b> <b>(<math>\sigma</math>)</b> <b>(%)</b>	<b>U<sub>system</sub> (3<math>\sigma</math>)</b> <b>(%)</b>	<b>k slope</b> <b>(pg/mL)<sup>-1</sup></b>	<b>LOD=3<math>\sigma</math>/kslope</b> <b>(pg/mL)</b>
CitH3	0.00093	0.00280	0.0032	0.87
IL-1 $\beta$	0.00176	0.0052784	0.0043	1.22
PCT	0.00197	0.00591	0.0036	1.64

## References

1. Hongsuk Nam; Sungjin Wi; Hossein Rokni; Mikai Chen; Greg Priessnitz; Wei Lu; Xiaogan Liang, *ACS Nano* **2013**, 7 (7), 5870-5881.
2. B. Pan; H. B. Alam; W. Chong; J. Mobley; B. Liu; Q. Deng; Y. Liang; Y. Wang; E. Chen; T. Wang; M. Tewari; Y. Li, *Sci. Rep.* **2017**, 7 (1), 8972. DOI 10.1038/s41598-017-09337-4.
3. Oriol Lopez-Sanchez; Dominik Lembke; Metin Kayci; Aleksandra Radenovic; Andras Kis, *Nat. Nanotechnol.* **2013**, 8, 497. DOI 10.1038/nnano.2013.100.
4. Dattatray J. Late; Bin Liu; H. S. S. Ramakrishna Matte; Vinayak P. Dravid; C. N. R. Rao, *ACS Nano* **2012**, 6 (6), 5635-5641. DOI 10.1021/nl301572c.
5. Jinsu Pak; Jingon Jang; Kyungjune Cho; Tae-Young Kim; Jae-Keun Kim; Younggul Song; Woong-Ki Hong; Misook Min; Hyoyoung Lee; Takhee Lee, *Nanoscale* **2015**, 7 (44), 18780-18788. DOI 10.1039/C5NR04836B.
6. Woong Choi; Mi Yeon Cho; Aniruddha Konar; Jong Hak Lee; Gi-Beom Cha; Soon Cheol Hong; Sangsig Kim; Jeongyong Kim; Debdeep Jena; Jinsoo Joo; Sunkook Kim, *Adv. Mater.* **2012**, 24 (43), 5832-5836. DOI doi:10.1002/adma.201201909.
7. Zongyou Yin; Hai Li; Hong Li; Lin Jiang; Yumeng Shi; Yinghui Sun; Gang Lu; Qing Zhang; Xiaodong Chen; Hua Zhang, *ACS Nano* **2012**, 6 (1), 74-80. DOI 10.1021/nl2024557.
8. Sylvia Underwood; Paul Mulvaney, *Langmuir* **1994**, 10 (10), 3427-3430. DOI 10.1021/la00022a011.
9. Ali Ghamin Al-Rubaye; Alexei Nabok; Anna Tsargorodska, *Procedia Technol.* **2017**, 27, 131-132. DOI <https://doi.org/10.1016/j.protcy.2017.04.057>.
10. Kristof Lodewijks; Willem Van Roy; Gustaaf Borghs; Liesbet Lagae; Pol Van Dorpe, *Nano Lett.* **2012**, 12 (3), 1655-1659. DOI 10.1021/nl300044a.
11. Seung-Woo Lee; Kyeong-Seok Lee; Junhyoung Ahn; Jae-Jong Lee; Min-Gon Kim; Yong-Beom Shin, *ACS Nano* **2011**, 5 (2), 897-904. DOI 10.1021/nl102041m.

12. A. Horrer; J. Haas; K. Freudenberger; G. Gauglitz; D. P. Kern; M. Fleischer, *Nanoscale* **2017**, *9* (44), 17378-17386. DOI 10.1039/C7NR04097K.
13. Mollye Sanders; Yongbin Lin; Jianjun Wei; Taylor Bono; Robert G. Lindquist, *Biosens. Bioelectron.* **2014**, *61*, 95-101. DOI <https://doi.org/10.1016/j.bios.2014.05.009>.
14. Feng Hao; Peter Nordlander; Yannick Sonnefraud; Pol Van Dorpe; Stefan A. Maier, *ACS Nano* **2009**, *3* (3), 643-652. DOI 10.1021/nn900012r.
15. C. L. Nehl; H. Liao; J. H. Hafner, *Plasmon resonant molecular sensing with single gold nanostars*. SPIE: **2006**; Vol. 6323, p 8.
16. Amane Shiohara; Judith Langer; Lakshminarayana Polavarapu; Luis M. Liz-Marzán, *Nanoscale* **2014**, *6* (16), 9817-9823. DOI 10.1039/C4NR02648A.